ACS OMEGA

http://pubs.acs.org/journal/acsodf

Article

ZSM-5 Catalysts for MTO: Effect and Optimization of the Tetrapropylammonium Hydroxide Concentration on Synthesis and Performance

Mohammed A. Sanhoob, Abuzar Khan,* and Aniz Chennampilly Ummer*

Cite This: *ACS Omega* 2022, 7, 21654–21663

Read Online

ACCESS | Metrics & More | Article Recommendations

ABSTRACT: Light olefin production from methanol using various zeolite catalysts has industrial and economic importance considering the growth of the petrochemical market. Zeolites are generally synthesized using various organic templates as structure-directing agents (SDAs). In this study, synthesis of a series of ZSM-5 zeolites was performed systematically using the microwave-assisted crystallization method, and these samples were analyzed in detail to understand the effect of the SDA concentration. Powder diffraction, N_2 adsorption, scanning electron microscopy, ammonia adsorption desorption, and ^{27}Al and ^{29}Si NMR spectroscopies were used for the characterization. The organic SDA tetrapropyl ammonium hydroxide ($TPAOH/SiO_2$ mole ratio = 0.0500) is found to have an optimum concentration against the silica precursor for achieving the highest crystallinity, suitable morphology, ideal pore size, effective pore volume, and tuned microporous/mesoporous area. For samples with a template concentration ratio of 0.050 or higher, ^{29}Si and ^{27}Al NMR data revealed the presence of an intact ZSM-5 structure. Using a fixed bed reactor at 500 °C and atmospheric pressure, the catalytic performance of the selected catalysts from the series is investigated for the methanol-to-olefin conversion reaction. The sample with the highest crystallinity showed the best conversion, selectivity toward light olefins, and time on stream stability. It is also worth noting that the highest crystallinity, micropore area, and micropore volume are reached for the optimum value rather than the highest template concentration. This allows for a reduction in the template concentration and a move closer to a synthesis pathway benign to environment and economics.

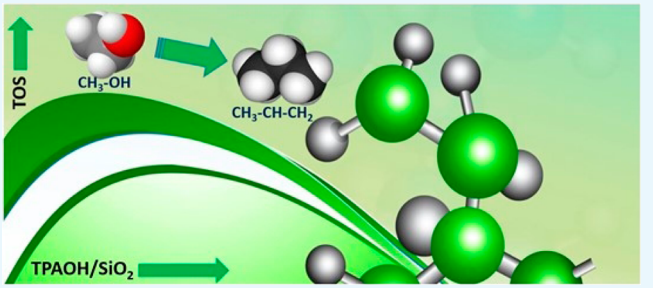

1. INTRODUCTION

Plastics are versatile materials with amazing properties like corrosion resistance, low-cost, light-weight, and ease of molding, to name a few. Plastics have captured a wide spectrum of consumer markets since 1950, with yearly production reaching 368 MT in 2019.[1] Plastic manufacture and processing might account for 20% of world petroleum consumption by 2050, according to projections.[2] Lower olefins are the principal raw material for plastics, and their synthesis is based on the cracking of naphtha feedstock from refineries.[3] The depletion of fossil fuels continues to be alarming, and the hunt for alternate sources has become a possible imperative. The prospect of manufacturing methanol either utilizing fossil fuels or renewable sources drew attention to the conversion of methanol to olefins.[4] The manufacture of olefins from methanol has advanced to commercial units (UOP/Norsk technology, Lurgi MTP method, D-MTO-Dalian Institute of Chemical Technology).[5,6]

Methanol is converted to olefins in a stoichiometric manner. Methanol is first dehydrated to dimethyl ether (DME), which is then dehydrated further to olefins, paraffins, and certain cyclic products.[7] High methanol conversion is seen over zeolite catalysts such as ZSM-5 and SAPO-34 at 400 °C and atmospheric pressure due to high reactivity.[8] The eight-ring (3.8 × 3.8A) cage like structured SAPO-34 allows the reaction to progress between hydrocarbons and methanol or DME molecules inside these cages. ZSM-5 zeolites[9] with straight (5.3 × 5.6A) and sinusoidal (5.1 × 5.5A) 10-ring channels having strong acid sites enhance the selectivity of propylene by means of olefin methylation and cracking reactions.[10] Furthermore, due to the limited reaction space inside the pores, coke production is limited to only the external surfaces.[11] Together with these advantages, the wide availability and possibilities of tuning the properties of ZSM-5[12] brought more attraction for ZSM-5 zeolites for the

Received: March 15, 2022
Accepted: June 6, 2022
Published: June 15, 2022

methanol-to-olefin application. Porosity,[13] acidity,[14−17] crystallite, and particle size[8,18−20] are some of the major physicochemical properties discussed in the literature that affect the reaction pathways and product selectivity of the methanol-to-olefin reaction.

In order to achieve these properties, various methods are being practiced and reported in the literature[21] for the synthesis of ZSM-5 zeolites. Organic templates or structure-directing agents (SDAs) play an important role even though efforts for template-free synthesis date back to the 1980s.[22] However, the recent interest toward green synthesis methods[23] calls for reducing these harmful chemicals used to prepare different aluminosilicates. Researchers make various efforts to eliminate the usage of SDAs,[24,25] eliminate solvents,[26] minimize use of solvents,[27] and recycle[28] solvents during the ZSM-5 synthesis without compromising on product yield and quality. Bukhari et al.[29] published an optimal template concentration for SBA-15 in 2017 in order to obtain a well-ordered structure that is favorable for CO_2 reforming of methane.

Only a few studies are found in our literature survey on reducing the SDA concentration in ZSM-5 synthesis. Alipour et al.[30] compiled some previous reports to show that pH and template concentration play a significant role in determining the crystallinity. Fouad et al.[31] minimized the template to the silica mole concentration to 0.215 to synthesize ZSM-5 zeolites. Chen et al.[32] studied the effect of varying NaOH concentrations on ZSM-5 properties and their catalytic performance for the methanol-to-propylene reaction using CTAB as the template. There exists a tradeoff between the minimal use of non-green chemicals and preserving the desired properties of the target materials during the synthesis step. This has to be experimented and evaluated typically to understand the structure−activity relationship depending on the application. This research aims to understand and optimize the least minimum requirement of SDA to generate ZSM-5 material and their performance in the methanol-to-olefin reaction.

2. EXPERIMENTAL SECTION

2.1. Catalyst Synthesis. Cost-effective ZSM-5 with Si/Al ratio of 50 was synthesized under microwave irradiation with the following chemical sources without further purification: (i) colloidal silica (40 wt % suspension in H_2O, LUDOX HS-40, Sigma-Aldrich), (ii) aluminum sulfate octadecahydrate [$Al_2(SO_4)_3{\cdot}18H_2O$, Acros], (iii) tetrapropylammonium hydroxide (TPAOH, 1.0 M in H_2O, Sigma-Aldrich), and (iv) sodium hydroxide (NaOH, Panreac). All synthesis parameters were kept constant except for the TPAOH/SiO_2 ratio. In a typical synthesis, sodium hydroxide (0.346 g) was dissolved in 38.5 g of deionized water (DI) water. The aluminum sulfate octadecahydrate (0.961 g) was added to the sodium hydroxide solution and aged for a few minutes until the complete dissolution of the aluminum content. Different amounts of TPAOH solution were added to the resulting solution to synthesize ZSM-5 zeolite with different TPAOH/SiO_2 ratios. The ratio of TPAOH/SiO_2 varied between 0.100 and 0.00625. Finally, colloidal silica (13.0 g) was added to the synthesis mixture. The solution was aged for 5 min to assure the homogeneity of the solution. After that, the synthesis mixture was transferred to 100 mL Teflon bottle and placed in the microwave (MicroSYNTH). The synthesis mixture was treated at 180 °C, and the stirring speed was maintained at 30%. The synthesis mixture was heated from room temperature to 180 °C in 5 min. Then, the temperature was dwelled for 90 min at 180 °C. After the completion of the synthesis, the sample was self-cooled, and the catalytic products were collected using the high-speed centrifuge. The product was collected and washed thoroughly with double distilled water to reduce the pH to ∼8. The synthesized samples were named as following: KM1 (TPAOH/SiO_2 = 0.100), KM2 (TPAOH/SiO_2 = 0.075), KM3 (TPAOH/SiO_2 = 0.050), KM4 (TPAOH/SiO_2 = 0.025), KM5 (TPAOH/SiO_2 = 0.0125), KM6 (TPAOH/SiO_2 = 0.00625), and KM7 (TPAOH/SiO_2 = 0.0).

2.2. Characterization. The chemical compositions (Si and Al) of the synthesized samples were determined using Horiba Ultima-2 ICP-OES calibrated against respective metal standards. Catalyst samples were digested using the HCl/HNO_3 mixture, extracted to aqueous solution, and analyzed, and Si/Al ratios are reported.

An X-ray diffractometer (XRD, Miniflex from Rigaku) equipped with Cu Kα radiation (λ = 0.15406 nm) was utilized to screen the phase purity and crystallinity of the synthesized ZSM-5 zeolite samples. The samples were characterized with a scanning step size of 0.02° and a scanning speed of 3° min^{-1}. Relative intensity values are calculated using the peak heights of the highest intense peak for these samples, at 2θ = 23.12. The sample with the highest peak intensity is kept as a reference to calculate the relative intensity values of the other samples. Field-emission scanning electron microscopy was used to examine the particle size and shape (FE-SEM, LYRA 3 Dual Beam, Tescan). Thermogravimetric analysis is carried out using the SDT-Q600 TA machine by loading 10 mg of each sample (100 °C dried) at 5 °C/min ramping up to 700 °C in the air atmosphere.

MAS NMR spectra were utilized to identify the zeolite coordination system of cost-effective ZSM-5 zeolite samples. The higher-resolution ^{29}Si MAS NMR and ^{27}Al MAS NMR spectra were analyzed using a JEOL ECA-600 spectrometer (14.1 T) equipped with an additional 1 kW power amplifier. ^{29}Si MAS NMR analysis was executed with a pulse width of 4.1 μs and 10,000 scans. The spinning rate and relaxation delay at a resonance frequency of 119.2 MHz were kept at 15 kHz and 30 s, respectively. On the other hand, solid-state ^{27}Al MAS NMR spectra of cost-effective ZSM-5 zeolite samples were evaluated at a pulse width of 3.25 μs and 4000 scans. The experiment was carried out at a spinning rate and relaxation delay of 15 kHz and 0.1 s, respectively. The resonance frequency was kept at 156.4 MHz. The chemical shift for ^{27}Al MAS NMR analysis was referenced to $AlNH_4(SO_4)_2{\cdot}12H_2O$ at −0.54 ppm. However, the chemical shift for ^{29}Si MAS NMR was referenced to polydimethylsilane at 34.12 ppm.

The textural properties of the cost-effective ZSM-5 zeolite were determined by the N_2 physisorption experiment (ASAP2020, Micromeritics). Prior to the measurement, the catalysts were degassed at 350 °C for 6 h to remove the moisture and impurities under vacuum and later flushed with an inert gas before transferring into the sample tube. After taking the weight measurement of the sample, the sample tube was transferred to the analysis port and degassed for the second time prior to the analysis at 350 °C for 2 h. The adsorption/desorption isotherms were then evaluated in a liquid nitrogen bath at 77 K.

The strength of zeolite acidity of the cost-effective ZSM-5 zeolite samples was analyzed using temperature-programmed desorption of ammonia (NH_3-TPD, MicrotracBEL). The

https://doi.org/10.1021/acsomega.2c01539
ACS Omega 2022, 7, 21654−21663

Table 1. Structural and Morphological Properties of Zeolites Synthesized with Different TPAOH Concentrations[a]

		weight loss			results from XRD data				
sample name	TPAOH/SiO_2	$W_{L\text{-}300}$	$W_{L\text{-}550}$	Si/Al ratio	I/I_o	2θ	Cry_S	d value	S_A
KM1	0.100	1.6	8.3	51.1	81.11	23.177	283.53	3.834	7.5
KM2	0.075	1.4	7.8	50.4	88.82	23.158	504.85	3.837	6.0
KM3	0.050	2.0	9.2	50.8	100.0	23.270	422.08	3.819	5.0
KM4	0.025	1.8	7.9	49.3	24.32	23.135	414.26	3.841	9.2
KM5	0.0125	2.5	8.5	50.1	20.81	23.124	612.89	3.843	
KM6	0.00625	1.4	10.1	49.8	14.75	23.131	435.91	3.841	
KM7	0	2.0	9.3	51.7					

[a] I/I_o—ratio of intensities of peaks at angle 2θ of the XRD profile. Cry_s—crystallite size values calculated from XRD data, Å. S_A—particle size calculated from SEM analysis, μm. $W_{L\text{-}300}/W_{L\text{-}550}$—% weight loss from TGA analysis in the ranges of 100−300 and 300−550 °C, respectively.

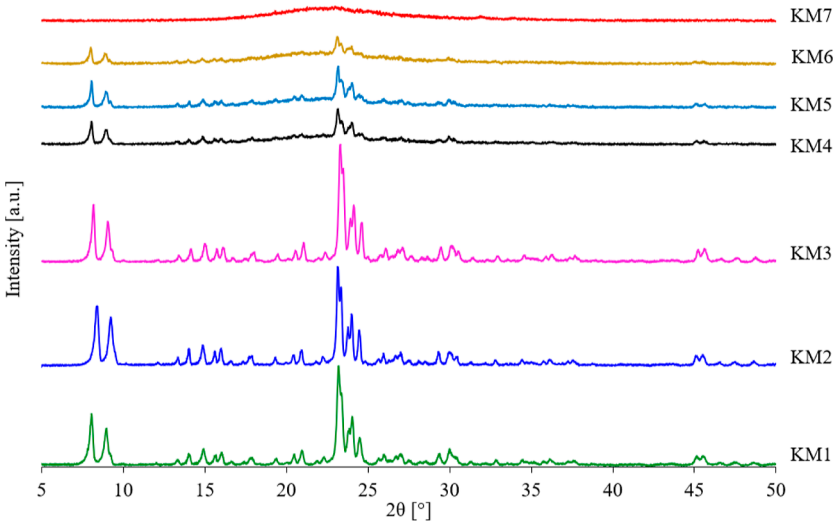

Figure 1. X-ray diffraction patterns of the zeolites synthesized using different TPAOH concentrations.

zeolite sample (about 50 mg) was pre-treated at 550 °C in the presence of continuous flow of helium gas for 60 min at 50 mL min^{-1}. After that, the sample was cooled to 100 °C followed by the adsorption of the NH_3 mixture for 30 min (10% NH_3 in helium, 50 mL min^{-1}). The physiosorbed gases were flushed with helium gas for 45 min with a helium flow rate of 30 mL/min. Finally, the sample was heated to 650 °C at a constant heating rate of 10 °C min^{-1} to desorb the NH_3 from the sample, and simultaneously, the TPD signal was monitored by a thermal conductivity detector (TCD).

2.3. Catalytic Evaluation. The catalytic performance of the cost-effective MFI (mordenite framework inverted) zeolite samples was evaluated in the catalytic conversion of methanol to olefin. All catalytic evaluations were evaluated with a catalyst weight of 100 mg with a pellet size of 100−299 μm in a fixed bed reactor with a reaction temperature of 500 °C and at atmospheric pressure. Methanol (purity ≥99.9% Aldrich) was fed to the reactor with a weight hourly space velocity (h^{-1}) of 4.75. The reaction was continued for a duration where the catalyst under evaluation showed a significant drop in light olefin formation, which is the desired product. Hence, the reaction time varies from 5 to 1 h for the best and worst-performing catalysts, respectively. Helium gas was employed as a carrier gas, and its flow rate was maintained at 18.6 mL min^{-1}. The catalytic products were analyzed by a gas chromatograph with a flame ionization detector packed with HP-PLOTQ (length 30 m, I.D. 0.53 mm, and thickness 5.0 μm) and a TCD packed with MS-13X (45/60, 9ft, 1/8″). Conversion is calculated from the concentration of unreacted methanol collected along with the product, and product distribution is calculated using the following equation:

$$\text{product distribution of } A = \frac{n_A}{n_{total} - n_{methanol}} \times 100\%$$

where n_A is the number of moles of product A formed, n_{total} is the total number of moles of all products formed, and $n_{methanol}$ is the number of moles of unreacted methanol.

3. RESULTS AND DISCUSSION

3.1. Elemental and X-ray Diffraction Analyses. All the catalyst samples prepared in this work were analyzed for metal contents, viz., Si and Al using ICP-OES, and the Si/Al ratios are reported in Table 1. Si/Al ratios of all the samples are well within the targeted value with ±5% maximum deviation, showing that difference in the TPAOH concentration does not alter the metal ratio incorporated into the framework. From TGA analysis, it is observed that beyond 550 °C, there is no weight loss and confirmed 550 °C as calcination temperature for all samples. The initial weight loss below 300 °C might be due to bound water, and 300−550 °C represents the weight loss associated with the decomposition of organic templates left and also the conversion of metal hydroxides to oxides.[33] One of the critical characterization methods in zeolite synthesis is to analyze the X-ray diffraction profile to match it with the respective reported standard peak profile of the material. The X-ray diffraction patterns of all the synthesized samples are

https://doi.org/10.1021/acsomega.2c01539
ACS Omega 2022, 7, 21654−21663

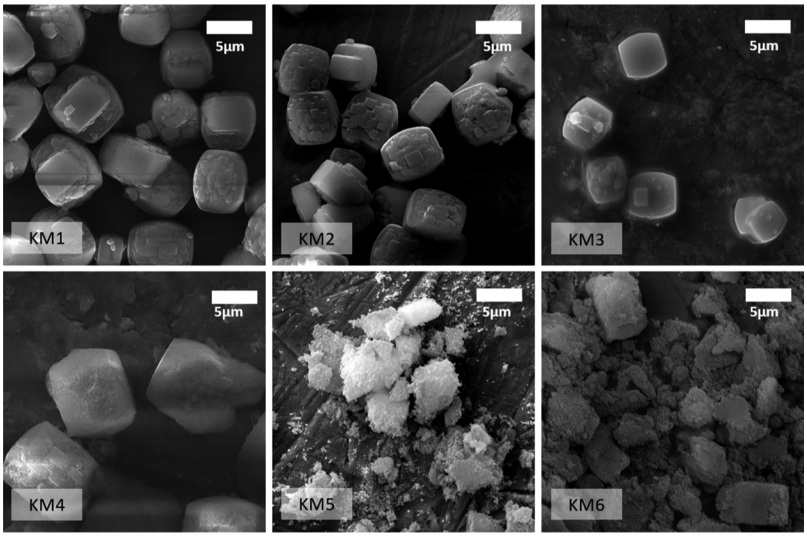

Figure 2. SEM images of the zeolite synthesized with different TPAOH concentrations.

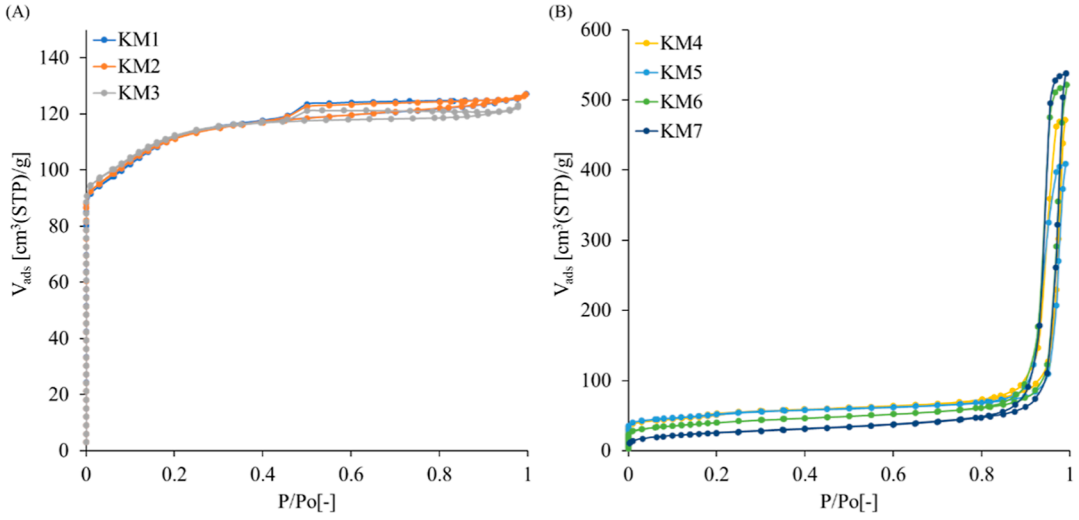

Figure 3. (A, B) BET isotherm of MFI zeolites synthesized with different TPAOH concentrations.

overlaid in Figure 1. All the catalysts except KM7 (TPAOH/SiO_2 = 0.00) are matching the characteristic peaks of pure ZSM-5 (PDF no. 44-0003), as reported in the literature[34] indicating the material purity. The characteristic peaks are well identified at 2θ positions of 7.92, 8.80, 14.78, 23.10, 23.90, and 24.40. It is well known that SDAs play a vital role in the formation of the zeolite structure during the synthesis step. The formation of the zeolite phase is generally impossible under the used experimental conditions in the absence of SDAs, and hence, the amorphous nature of KM7 is expected. From Figure 1, it is clearly understood that the peak intensity keeps reducing and diminishes as we move from higher to lower SDA concentrations among the samples. A significant drop in peak intensity occurred beyond KM3 (TPAOH/SiO_2 = 0.050), showing that it is practically possible to minimize the SDA concentration up to this level. This observation is in agreement with the results reported by Karimi et al.[35] who have reported that a template ratio of 0.058 is found to be the lowest best even though their synthesis time is higher and is in the range of 100 h. The crystallization time in all our experiments was constant (90 min), and the slurry pH was 13 ± 0.2; hence, we do not see such observations, as reported by Alipour et al.[30] The relative intensity is highest for KM3 sample, as calculated from the highest intense peak (2θ around 23.15), and hence, we fixed its I/I_o as 100 to compare other samples. The crystallite size values, d spacing, 2θ positions, and the relative intensities are included in Table 1 for convenience. The minor shift in 2θ peak positions and d values can be understood due to the slight expansion of the zeolite unit cells.[34]

3.2. SEM Analysis. The SEM images of KM1, KM2, and KM3 revealed a regular, well-defined, and prismatic morphology with smooth surfaces, confirming the formation of crystalline ZSM-5 phase with good crystallinity, as shown in Figure 2. We have ruled out KM7 being a totally amorphous material, as evidenced by XRD analysis. Beyond KM3 (TPAOH/SiO_2 = 0.0500), the crystallization strength decreased dramatically, and the samples exhibited a primarily amorphous character, according to X-ray diffraction data. The crystallization process is also not complete, as evidenced by the hazy background in SEM images of KM3, KM4, KM5, and KM6.

The particle size values go down with decrease in the SDA concentration until TPAOH/SiO_2 ratio of 0.0500. Beyond this

https://doi.org/10.1021/acsomega.2c01539
ACS Omega 2022, 7, 21654−21663

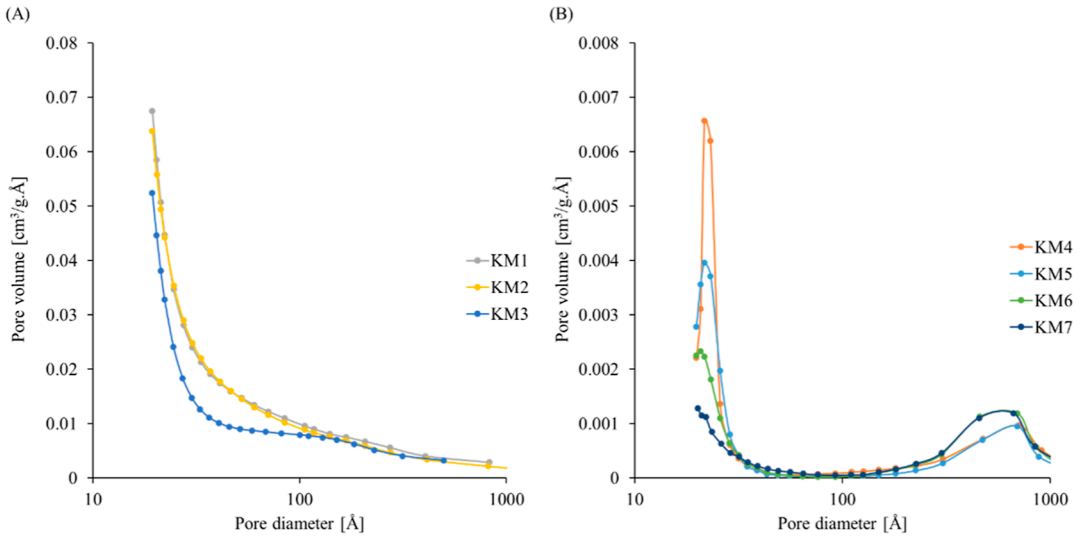

Figure 4. (A, B) Pore volume vs pore diameter plots of MFI zeolites synthesized with different TPAOH concentrations.

value, the particle morphology turns to irregular and ill-defined morphology. It also tends to increase the particle size, as reported by many earlier researchers,[36] and we also observed the same while moving from KM1 to KM3. However, there is a minimum SDA concentration needed for the crystallization to occur and ZSM-5 structure to form.

3.3. N_2 Adsorption Analysis. N_2 adsorption results help clearly differentiate between the crystalline/amorphous materials from the shape of isotherm plots, as shown in Figure 3. Samples KM1, KM2, and KM3 have perfect microporous type-1 isotherm shape, whereas KM4, KM5, and KM6 showed type-IV shape with the hysteresis loop.[37] The hysteresis loop could be due to the delayed desorption of adsorbed N_2 from the inter-particle voids formed between the crystallites. In the former set, a significant adsorption occurred within 0.001 P/P_o values. The latter set demonstrated significant adsorption coupled with a hysteresis loop between P/P_o of 0.8 and 1.0. Figure 4 shows the deflection in the pore volume values when we move from TPAOH/SiO_2 of 0.0500 (KM3) to TPAOH/SiO_2 of 0.0250 (KM4) and beyond.

Brunauer–Emmett–Teller (BET) surface area values showed notable difference, viz., from ∼400 to ∼180 m^2/g when we change the TPAOH/SiO_2 ratio from 0.050 to 0.025, as shown in Table 2. This change is caused due to rapid drop in micropore volumes and surface area as we move from 0.050 to 0.025 TPAOH/SiO_2 mole ratios. Total pore volume values increased dramatically in response to the decrease in the SDA ratio; however, this was offset by an increase in mesoporous volumes. The mesoporous volumes could be attributed to the inter-particle voids that arose from adjacent nano-crystallites present in the amorphous and semi-amorphous samples, as reported earlier.[38] The poor micropore volume and micropore surface area for KM7 shows that this is no more a zeolite but rather an amorphous aluminosilicate only.

The proper balance between mesopore and micropore volumes of ZSM-5 zeolites are appreciably responsible for various catalytic properties[13] including the title reaction.

3.4. NH_3 TPD. The total acidity of the samples prepared in this study is the highest for KM1 (TPAOH/SiO_2 = 0.1000) and the lowest for KM6 (TPAOH/SiO_2 = 0.00625). KM1 has a total acidity of 0.262 mmol/g, whereas KM6 contains only 0.061 mmol/g. We have not analyzed KM7 since it is a completely amorphous material, as observed from XRD analysis. As demonstrated in Table 3, the total acidity pattern follows the order KM1 > KM2 > KM3 > rest of the samples. According to the NH_3-TPD study results in Figure 5, KM1 has the highest strong acidity. Both strong and weak acidity are significantly low for all the samples through KM4 to KM6.

The acidity values follow the same pattern as the N_2 adsorption investigation and support our results and explain why the products generated beyond KM3 is significantly different. In the experimental settings detailed in this work, the presence of a minimum SDA concentration is essential for zeolite crystallization to occur. As the sample becomes more crystalline, the T_{max} of both strong and weak acid site peaks

Table 2. N_2 Adsorption Results for MFI Zeolites Synthesized with Different TPAOH Concentrations[a]

sample details	S_{BET}	S_{micro}	S_{extr}	V_{total}	V_{micro}	V_{meso}
KM1	397	209	189	0.194	0.089	0.105
KM2	399	230	169	0.194	0.097	0.097
KM3	400	240	163	0.187	0.102	0.086
KM4	177	47	130	0.355	0.022	0.333
KM5	182	72	110	0.320	0.032	0.289
KM6	142	42	100	0.451	0.019	0.433
KM7	90	9	81	0.405	0.003	0.401

[a] S_{BET}—BET surface area (m^2/g). S_{micro}—micropore area (m^2/g). S_{extr}—external area (m^2/g). V_{total}—BJH des. Total pore volume (cm^3/g). V_{micro}—micropore volume (cm^3/g). V_{meso}—mesopore volume (cm^3/g).

Table 3. Acidity Results of MFI Zeolites Synthesized with Different TPAOH Concentrations

	NH_3-TPD acidity (mmol/g)		
sample details	weak acidity	strong acidity	total acidity
KM1	0.107	0.155	0.262
KM2	0.103	0.134	0.237
KM3	0.094	0.126	0.220
KM4	0.040	0.065	0.105
KM5	0.032	0.066	0.098
KM6	0.038	0.023	0.061

https://doi.org/10.1021/acsomega.2c01539
ACS Omega 2022, 7, 21654−21663

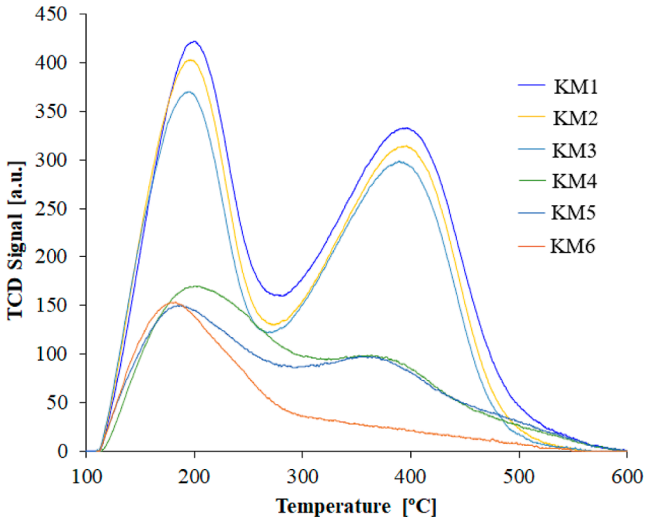

Figure 5. NH_3 desorption peak profiles of MFI zeolites synthesized with different TPAOH concentrations.

moves to the high-temperature side. For the crystalline set, the T_{max} of mild and strong acidity peaks is approximately 200 and 400 °C, respectively, but for the less crystalline sample set, they are around 175 and 375 °C.

3.5. MAS NMR. The prepared zeolite samples were analyzed for ^{27}Al MAS NMR and ^{29}Si MAS NMR to understand the coordination number of Al and Si ions to the zeolite framework (Figure 6), their environment with the heteroatoms present, their presence as extra framework ions, and to correlate it with the acidity of zeolites. In ^{27}Al NMR (Figure 6A), the presence of a peak around 53 ppm represents the tetrahedral coordination (framework ions), whereas the peak around 0 ppm indicates the octahedral extra-framework Al ions. For KM1, KM2, and KM3, the sharp and high intensity peak at 53 ppm reveals strong tetrahedral coordination of Al ions onto the ZSM-5 framework. Other samples, such as those with a lower TPAOH concentration (TPAOH/SiO_2 ratio below 0.050), had a broad band at 53 ppm, indicating poor tetrahedral coordination of Al ions to the ZSM-5 structure. For these samples, the peak at 0 ppm is negligible or absent, showing that Al ions fail to coordinate by the octahedral way in these samples. The spectra show no peak around 25 and 13 to −17 ppm, confirming that no aluminum oxide ions are present in the extra framework in any of the prepared samples. Aluminum ions play a key role in Brønsted acidity, and the target Si/Al ratio is the same for all the samples prepared in this study.

The difference in the coordination mode of Al ions in the ZSM-5 framework critically alters the acidic properties of the samples, especially the Brønsted acidity. The tetrahedral to octahedral coordination percentage ratios of KM1, KM2, and KM3 are 94.34, 94.87, and 96.11, respectively, calculated from the relative intensities of 53 and 0 ppm peaks.

^{29}Si MAS NMR analysis provides information about the silica substitution onto the ZSM-5 framework and its coordination with the surrounding heteroatoms, which are Al ions in this case. There are various well-known individual resonance peaks around 100−120 ppm representing Q^2, Q^3, and Q^4 units.[39] Some of these have been ascribed to Si(4Si) sites (−110 ppm), Si(3Si,1Al) sites (−103 to −108 ppm), and Si(2Si,2Al) sites (below 100 ppm).[40] However, in this study, we do not deconvolute these peak profiles to analyze them in detail. Even though the desired Si/Al ratios were the same in all the samples, the low intensity bands for samples with TPAOH concentrations <0.050 show feeble Si-substitution onto the ZSM-5 structure (Figure 6B).

3.6. Catalytic Evaluation. The catalysts were evaluated for their performance in a fixed bed reactor at 500 °C and atmospheric pressure. The initial product analysis is evaluated after 12 min from starting of the reaction. In the initial examination, all of the crystalline samples perform well in terms of methanol conversion and selectivity, with the exception of KM6, which does not crystallize to the ZSM-5 structure, as evidenced by characterization data. At the same time, KM6 has the smallest micropore area and micropore volume, together with higher mesopore volume, which might lead to rapid deactivation and failure. During the methanol conversion process, a significant amount of carbon develops and clogs the catalyst pore, deactivating the catalyst over time.[41] The quantity and accessibility of the active site decide the time up to which the reaction proceed giving the desired products. Some earlier studies[13,42] reported the advantages on product selectivity, especially on ethylene and propylene once the catalyst get pre-coked to certain levels.

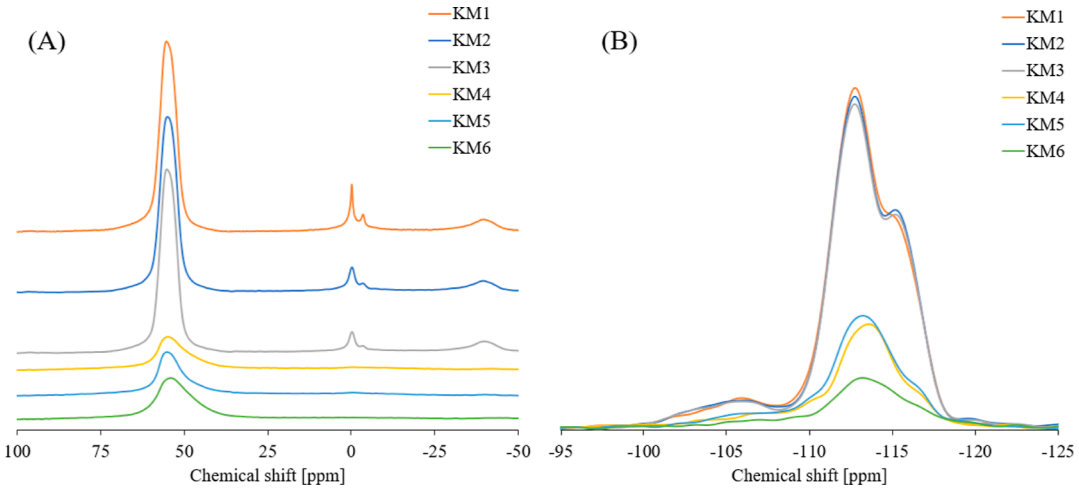

Figure 6. (A) ^{27}Al MAS NMR and (B) ^{29}Si MAS NMR of MFI zeolites synthesized with different TPAOH concentrations.

https://doi.org/10.1021/acsomega.2c01539
ACS Omega 2022, 7, 21654−21663

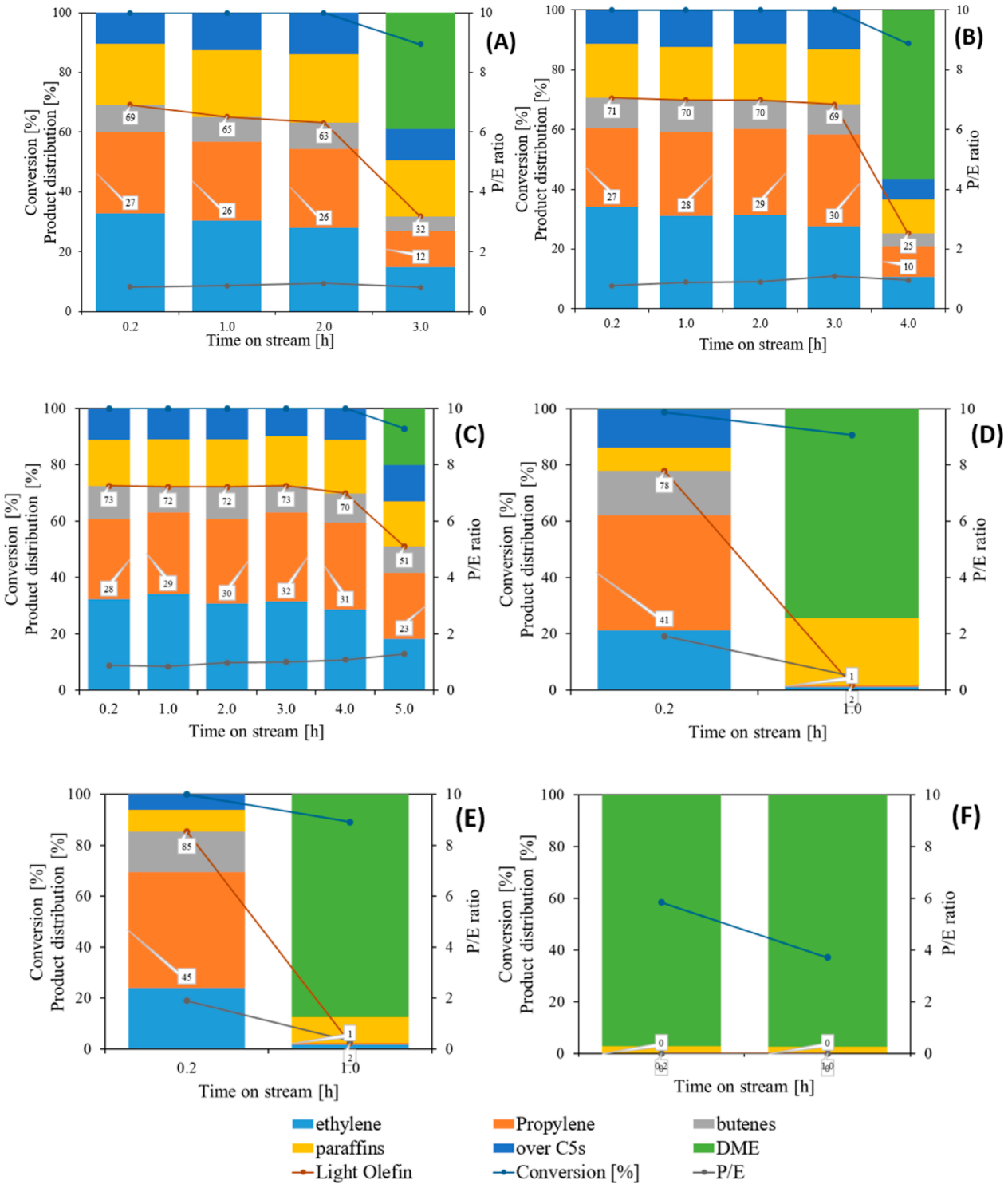

Figure 7. Catalytic performance results of MFI zeolite samples prepared with different TPAOH concentrations at 450 °C and an He flow rate of 18.6 mL/min. (A) KM1, (B) KM2, (C) KM3, (D) KM4, (E) KM5, and (F) KM6.

The formation of DME from methanol occurs via the dehydration step[43] and can occur even on the γ-Al_2O_3 alumina catalyst, though it gets deactivated quickly by the formed water molecules.[44] During the methanol-to-olefin reaction, DME is produced even at 200−300 °C. Hence, the formation of DME on the KM6 catalyst, which does not possess ZSM-5 structure, is expected. During our study, whenever DME starts to form in the product at significant amounts and the total light olefin content dropped below 30%, we discontinued the reaction. The reaction mechanism of the methanol-to-olefin reaction is discussed in various reports in details.[13]

KM4 and KM5 samples produced a variety of desired products depending on the degree of crystallinity and the presence of the partial ZSM-5 structure but for transient short duration only. This can be understood in terms of immediate consumption of available micropores and active sites, given their high accessibility seen from their high pore volume. Once these sites are utilized and fully deposited with coke, no further

https://doi.org/10.1021/acsomega.2c01539
ACS Omega 2022, 7, 21654−21663

formation of olefins and paraffins might happen[45] from these catalysts unless simultaneous coke burning also happened to retain active sites. In such cases, it may lead to selectivity changes, as discussed earlier.[42]

Higher BET surface area values and higher pore volume show improved diffusion possibility of the reactants through the zeolite channels. However, this should be accompanied together with minimum micropore volume for the reaction to proceed smoothly over time. This is also supported by the NH_3-TPD results, owing to the requirement of optimized acidic and active site density across the catalyst surface.[46] The acid site concentration per unit surface area of the catalyst is critical for the diffusion of reactants and products through the zeolite channels. As seen in the SEM results, the smaller and discrete particle size of KM3 combined with a narrow particle size distribution must have contributed to better contact time and quick diffusion of the reactant. The best-performing catalyst has the highest micropore area and the lowest crystallite size, which is reported in earlier studies[47] for this reaction.

When comparing ^{27}Al NMR and ^{29}Si NMR data, it is clear that Si incorporation is similar for KM1, KM2, and KM3 samples, but the tetrahedral and octahedral coordination of Al ions differs. The I/I_o ratio from XRD analysis follows the order KM3 > KM2 > KM1, as depicted in Table 1. This clearly shows the difference in substitution of Al ions to the framework and extra framework sites and leads to differences in their Bronsted acidity, as reported in the literature.[41] The type and concentration of these acidic sites play an important role in deciding their catalytic performances.

Product distribution and conversion values are plotted in Figure 7 for maximum of 5 h duration depending on each sample performance. The KM3 sample produced the highest ethylene and propylene, with 34.1% and 28.8%, respectively, at the 5th hour, respectively. The selectivity toward ethylene and propylene is affected by several parameters like Si/Al ratio, Bronsted and Lewis acidity values, presence of Al ions in the tetrahedral/octahedral position on the framework, and so on, as reported in the literature.[48,49] During initial deactivation of all the catalysts, ethylene formation diminished faster than propylene formation. The hydrocarbon speciation of all the products formed during the reaction over KM1, KM2, and KM3 is listed in Table 4.

Among KM1, KM2, and KM3 samples, the catalytic conversion during the initial hours is similar, whereas the desired product selectivity dropped quickly for KM1 and KM2 compared to KM3. During the initial reaction hours, DME was not seen among the product for crystalline sample sets, say KM1, KM2, and KM3. However, DME become the major single product for KM1 and KM2, and the total light olefin count reduced to 32 and 25% after 3rd and 4th hour, respectively.

Figure 8 represents the graphical view of the trend of the productive time on stream over the catalysts prepared using different TPAOH/SiO_2 ratios.

Percentages of DME at 3rd and 4th hour for KM1 and KM2 are 40 and 60%, respectively. However for KM3, at 5th hour DME appeared as a product, but 51% of the product is still light olefins, proving this as the best catalyst in the series. The deactivation of KM2 faster by more than 1 h compared to KM3 in terms of olefin production. Moreover, the sudden drop in light olefin formation over KM2 shows that the type of coke formed over KM2 could be harder than that formed over KM3. This could be due to the high rate of carbon deposition. The final spent catalyst coke content will not help understand this effect, and it needs to monitor the formation of the coke content on the catalysts at each hour of the reaction. We have not performed such monitoring in this study. During the methanol-to-olefin process, the regeneration of soft coke is easier by adjusting the process parameters like temperature, as reported in the literature.[45]

Table 4. Detailed Hydrocarbon Analysis of Product Streams of Selected Catalysts

hydrocarbon product distribution, %	KM1	KM2	KM3
methane, C_1	14.39	9.03	10.29
ethylene, C_2=	30.40	31.28	34.17
ethane, C_2	0.72	0.75	0.71
propylene, C_3=	26.33	27.89	28.84
propane, C_3	4.14	5.62	4.23
isobutane, *i*-C_4	2.82	2.27	1.44
n-butane, C_4	0.03	0.08	0.08
C4 olefins, C_4=	8.43	10.73	9.12
isopentane, *i*-C5	5.08	5.03	4.46
n-pentane, C_5	0.96	0.80	0.00
C_{6+}	6.67	9.49	6.22
total percentage	100	100	100

4. CONCLUSIONS

In this paper, the synthesis, characterization, and catalytic performance evaluation of synthesized ZSM-5 samples are thoroughly addressed and examined. The physico-chemical characteristics of the ZSM-5 samples prepared using this method clearly demonstrated that in order to form a crystalline zeolite framework, a minimum concentration of SDAs is required. The products formed when the TPAOH concentration is more than 0.0500 TPAOH/SiO_2 mole ratio are regular, crystalline, and have the reported pantasil shape of ZSM-5 zeolite, as shown by powder XRD results. Crystallinity decreases below these concentrations, eventually resulting in amorphous material, which is the case in the absence of organic templates. The XRD results were supported by N_2 adsorption analysis, which revealed a clear distinction between crystalline and amorphous materials. From powder XRD, the most crystalline sample is not the one with the highest template concentration. The same trend is seen from the BET and BJH values of these samples. The highest crystalline sample was obtained with a TPAOH concentration of 0.0500, while the same sample also had the largest micropore volume and micropore surface area. The formation of the pantasil structure and its crystallinity were understood from SEM data that the TPAOH = 0.0500 batch produced aluminosilicate with a smaller particle size. The ammonia TPD of the crystalline samples does not differ significantly, but slight changes in porosity and micropore surface area, along with considerable variances in porosity and micropore surface area, result in performance differences. Characterization using ^{29}Si and ^{27}Al NMR became a confirmation tool to understand the ZSM-5 structure formation and the coordination environment of zeolite framework atoms. The catalytic performance of all the catalysts, except the fully amorphous one, has been carried out, and the results are well analyzed in this study. During the methanol-to-olefin reaction, the catalyst with highest crystallinity, micropore volume, micropore surface area, and higher

https://doi.org/10.1021/acsomega.2c01539
ACS Omega 2022, 7, 21654−21663

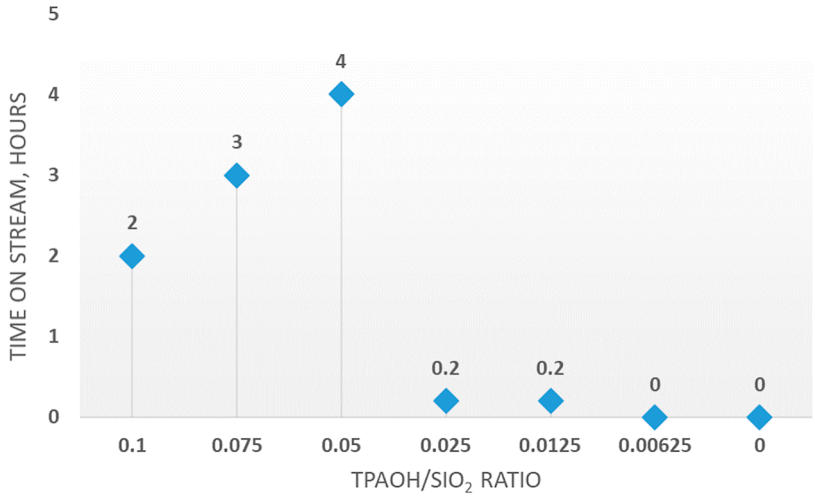

Figure 8. Graphical representation of time on stream vs TPAOH/SiO_2.

but optimal acidity displayed the best performance. During the reaction, this sample had the highest ethylene and propylene selectivity as well as the longest duration on stream stability. This research suggests that there is an optimum concentration for the organic template during the crystallization process, which should be tested in all synthesis methods, including commercial routes. These efforts are thought to help us get closer to a benign synthesis route that will protect our environment.

AUTHOR INFORMATION

Corresponding Authors

Abuzar Khan − *Interdisciplinary Research Center for Hydrogen and Energy Storage (IRC-HES), King Fahd University of Petroleum & Minerals, Dhahran 31261, Saudi Arabia;* orcid.org/0000-0001-9122-2247; Phone: +966-(13) 860 3642; Email: abuzar@kfupm.edu.sa

Aniz Chennampilly Ummer − *Interdisciplinary Research Center for Refining and Advanced Chemicals (IRC-CRAC), King Fahd University of Petroleum and Minerals, Dhahran 31261, Saudi Arabia;* orcid.org/0000-0002-3577-0713; Phone: +966-(13) 860 7576; Email: aniz.ummer@kfupm.edu.sa

Author

Mohammed A. Sanhoob − *Interdisciplinary Research Center for Hydrogen and Energy Storage (IRC-HES), King Fahd University of Petroleum & Minerals, Dhahran 31261, Saudi Arabia;* orcid.org/0000-0002-0574-5058

Complete contact information is available at: https://pubs.acs.org/10.1021/acsomega.2c01539

Notes

The authors declare no competing financial interest.

ACKNOWLEDGMENTS

The authors greatly acknowledge the research funding from the Deanship of Research Oversight and Coordination (DROC), King Fahd University of Petroleum and Minerals, Dhahran 31261, Saudi Arabia. The authors would like to acknowledge the Interdisciplinary Research Center for Hydrogen and Energy Storage (IRC-HES), and the Interdisciplinary Research Center for Refining Advanced Chemicals (IRC-RAC), King Fahd University of Petroleum and Minerals, Dhahran 31261, Saudi Arabia for hosting and supporting the research activities.

REFERENCES

(1) Panda, A. K.; Singh, R. K.; Mishra, D. K. Thermolysis of waste plastics to liquid fuelA suitable method for plastic waste management and manufacture of value added products-A world prospective. *Renewable Sustainable Energy Rev.* **2010**, *14*, 233−248.

(2) Lebreton, L.; Andrady, A. Future Scenarios of Global Plastic Waste Generation and Disposal. *Palgrave Commun.* **2019**, *5*, 6.

(3) Amghizar, I.; Vandewalle, L. A.; Van Geem, K. M.; Marin, G. B. New Trends in Olefin Production. *Engineering* **2017**, *3*, 171−178.

(4) Pirola, C.; Bozzano, G.; Manenti, F. Fossil or Renewable Sources for Methanol Production? In *Methanol*; Basile, A., Dalena, F., Eds.; Elsevier, 2018; Chapter 3, pp 53−93.

(5) Chen, Y.-H.; Hsieh, W.; Chang, H.; Ho, C.-D. Design and Economic Analysis of Industrial-Scale Methanol-to-Olefins Plants. *J. Taiwan Inst. Chem. Eng.* **2022**, *130*, 103893.

(6) Jasper, S.; El-Halwagi, M. A Techno-Economic Comparison between Two Methanol-to-Propylene Processes. *Processes* **2015**, *3*, 684.

(7) Gogate, M. R. Methanol-to-Olefins Process Technology: Current Status and Future Prospects. *Pet. Sci. Technol.* **2019**, *37*, 559−565.

(8) Jang, H.-G.; Min, H.-K.; Lee, J. K.; Hong, S. B.; Seo, G. SAPO-34 and ZSM-5 nanocrystals' size effects on their catalysis of methanol-to-olefin reactions. *Appl. Catal., A* **2012**, *437*−*438*, 120−130.

(9) Sanhoob, M. A.; Shafei, E. N.; Khan, A.; Nasser, G. A.; Bakare, I.; Muraza, O.; Al-Bahar, M. Z.; Al-Jishi, A. N.; Al-Badairy, H. H.; Ummer, A. C. Catalytic Cracking of *n*-Dodecane to Chemicals: Effect of Variable-Morphological ZSM-5 Zeolites Synthesized Using Various Silica Sources. *ACS Omega* **2022**, *7*, 10317−10329.

(10) Haw, J. F.; Marcus, D. M. Well-Defined (Supra)molecular Structures in Zeolite Methanol-to-Olefin Catalysis. *Top. Catal.* **2005**, *34*, 41−48.

(11) Bjørgen, M.; Svelle, S.; Joensen, F.; Nerlov, J.; Kolboe, S.; Bonino, F.; Palumbo, L.; Bordiga, S.; Olsbye, U. Conversion of Methanol to Hydrocarbons over Zeolite H-ZSM-5 : On the Origin of the Olefinic Species. *J. Catal.* **2007**, *249*, 195−207.

(12) Ummer, A. C.; Akhtar, M. N.; Alnaimi, E.; Ding, L.; Alasiri, H. S. Aromatization of Commercial Full Range Naphtha Over Modified Hierarchical ZSM-5 Catalyst. *ChemistrySelect* **2021**, *6*, 11541−11550.

(13) Olsbye, U.; Svelle, S.; Bjørgen, M.; Beato, P.; Janssens, T. V. W.; Joensen, F.; Bordiga, S.; Lillerud, K. P. Conversion of Methanol to Hydrocarbons: How Zeolite Cavity and Pore Size Controls Product Selectivity. *Angew. Chem., Int. Ed.* **2012**, *51*, 5810−5831.

(14) ZHANG, H.-r.; LIU, H.-y.; PAN, Q.-l.; LIU, H.-j.; SHEN, L.-z.; CUI, Y.; LIU, Y.-d.; ZHANG, T.; JIANG, Y.; GUO, Y. Modification of the acidic and textural properties of ZSM-5 zeolite by using double mineralizers in synthesis and its catalytic performance in the conversion of methanol to propene. *J. Fuel Chem. Technol.* **2018**, *46*, 967−976.
(15) Shamanaeva, I. A.; Yu, Z.; Utemov, A. V.; Wu, W.; Sladkovskiy, D. A.; Parkhomchuk, E. V. Role of Texture and Acidity of SAPO-34 in Methanol to Olefins Conversion. *Pet. Chem.* **2020**, *60*, 471−478.
(16) Bakare, I. A.; Muraza, O.; Yoshioka, M.; Yamani, Z. H.; Yokoi, T. Conversion of Methanol to Olefins over Al-Rich ZSM-5 Modified with Alkaline Earth Metal Oxides. *Catal. Sci. Technol.* **2016**, *6*, 7852−7859.
(17) Peng, Q.; Wang, G.; Wang, Z.; Jiang, R.; Wang, D.; Chen, J.; Huang, J. Tuning Hydrocarbon Pool Intermediates by the Acidity of SAPO-34 Catalysts for Improving Methanol-to-Olefins Reaction. *ACS Sustainable Chem. Eng.* **2018**, *6*, 16867−16875.
(18) Sugimoto, M.; Katsuno, H.; Takatsu, K.; Kawata, N. Correlation between the Crystal Zize and Catalytic Properties of ZSM-5 Zeolites. *Zeolites* **1987**, *7*, 503−507.
(19) Shiralkar, V. P.; Joshi, P. N.; Eapen, M. J.; Rao, B. S. Synthesis of ZSM-5 with Variable Crystallite Size and Its Influence on Physicochemical Properties. *Zeolites* **1991**, *11*, 511−516.
(20) Rownaghi, A. A.; Rezaei, F.; Hedlund, J. Yield of Gasoline-Range Hydrocarbons as a Function of Uniform ZSM-5 Crystal Size. *Catal. Commun.* **2011**, *14*, 37−41.
(21) Li, S.; Li, J.; Dong, M.; Fan, S.; Zhao, T.; Wang, J.; Fan, W. Strategies to Control Zeolite Particle Morphology. *Chem. Soc. Rev.* **2019**, *48*, 885−907.
(22) Dai, F.-Y.; Suzuki, M.; Takahashi, H.; Saito, I. Mechanism of Zeolite Crystallization without Using Template Reagents of Organic Bases. *Stud. Surf. Sci. Catal.* **1986**, *28*, 223−230.
(23) Devatha, C. P.; Thalla, A. K. Green Synthesis of Nanomaterials. In *Micro and Nano Technologies*; Mohan Bhagyaraj, S., Oluwafemi, O. S., Kalarikkal, N., Thomas, S., Eds.; Woodhead Publishing, 2018; pp 169−184.
(24) Nada, M. H.; Larsen, S. C. Insight into Seed-Assisted Template Free Synthesis of ZSM-5 Zeolites. *Microporous Mesoporous Mater.* **2017**, *239*, 444−452.
(25) Cheng, Y.; Wang, L.-J.; Li, J.-S.; Yang, Y.-C.; Sun, X.-Y. Preparation and Characterization of Nanosized ZSM-5 Zeolites in the Absence of Organic Template. *Mater. Lett.* **2005**, *59*, 3427−3430.
(26) Liu, Z.; Wu, D.; Ren, S.; Chen, X.; Qiu, M.; Liu, G.; Zeng, G.; Sun, Y. Facile One-Pot Solvent-Free Synthesis of Hierarchical ZSM-5 for Methanol to Gasoline Conversion. *RSC Adv.* **2016**, *6*, 15816−15820.
(27) Hartanto, D.; Iqbal, R. M.; Shahbihi, W. E.; Santoso, E.; Fansuri, H.; Iryani, A. Effect of H_2O/SiO_2 Molar Ratio on Direct Synthesis of ZSM-5 from Bangka's Kaolin Without Pretreatment. *Malaysian J. Fundam. Appl. Sci.* **2017**, *13*, 817−820.
(28) Pan, H.; Pan, Q.; Zhao, Y.; Luo, Y.; Shu, X.; He, M. A Green and Efficient Synthesis of ZSM-5 Using NaY as Seed with Mother Liquid Recycling and in the Absence of Organic Template. *Ind. Eng. Chem. Res.* **2010**, *49*, 7294−7302.
(29) Bukhari, S. N.; Chin, C. Y.; Setiabudi, H. D.; Vo, D.-V. N. Tailoring the Properties and Catalytic Activities of Ni/SBA-15 via Different TEOS/P123 Mass Ratios for CO_2 Reforming of CH4. *J. Environ. Chem. Eng.* **2017**, *5*, 3122−3128.
(30) Alipour, S. M.; Halladj, R.; Askari, S. Effects of the Different Synthetic Parameters on the Crystallinity and Crystal Size of Nanosized ZSM-5 Zeolite. *Rev. Chem. Eng.* **2014**, *30*, 289−322.
(31) Fouad, O. A.; Mohamed, R. M.; Hassan, M. S.; Ibrahim, I. A. Effect of Template Type and Template/Silica Mole Ratio on the Crystallinity of Synthesized Nanosized ZSM-5. *Catal. Today* **2006**, *116*, 82−87.
(32) Chen, H.; Wang, Y.; Meng, F.; Sun, C.; Li, H.; Wang, Z.; Gao, F.; Wang, X.; Wang, S. Aggregates of Superfine ZSM-5 Crystals: The Effect of NaOH on the Catalytic Performance of Methanol to Propylene Reaction. *Microporous Mesoporous Mater.* **2017**, *244*, 301−309.
(33) Hassanpour, S.; Taghizadeh, M.; Yaripour, F. Preparation, Characterization, and Activity Evaluation of H-ZSM-5 Catalysts in Vapor-Phase Methanol Dehydration to Dimethyl Ether. *Ind. Eng. Chem. Res.* **2010**, *49*, 4063−4069.
(34) Groen, J. C.; Peffer, L. A. A.; Moulijn, J. A.; Pérez-Ramírez, J. Mechanism of Hierarchical Porosity Development in MFI Zeolites by Desilication: The Role of Aluminium as a Pore-Directing Agent. *Chemistry* **2005**, *11*, 4983−4994.
(35) Karimi, R.; Bayati, B.; Charchi Aghdam, N.; Ejtemaee, M.; Babaluo, A. A. Studies of the Effect of Synthesis Parameters on ZSM-5 Nanocrystalline Material during Template-Hydrothermal Synthesis in the Presence of Chelating Agent. *Powder Technol.* **2012**, *229*, 229−236.
(36) Zhang, G.; Fan, Y.; Huang, J.; Wang, L.; Yang, C.; Lyu, M.; Liu, H.; Ma, Y. Decoupling Nucleation from Crystal-Growth for the Synthesis of Nanocrystalline Zeolites. *Dalton Trans.* **2020**, *49*, 7258−7266.
(37) Zhang, H.; Hu, Z.; Huang, L.; Zhang, H.; Song, K.; Wang, L.; Shi, Z.; Ma, J.; Zhuang, Y.; Shen, W.; Zhang, Y.; Xu, H.; Tang, Y. Dehydration of Glycerol to Acrolein over Hierarchical ZSM-5 Zeolites: Effects of Mesoporosity and Acidity. *ACS Catal.* **2015**, *5*, 2548−2558.
(38) Sing, K. S. W. Reporting Physisorption Data for Gas/Solid Systems with Special Reference to the Determination of Surface Area and Porosity (Recommendations 1984). *Pure Appl. Chem.* **1985**, *57*, 603−619.
(39) Luhmer, M.; d'Espinose, J. B.; Hommel, H.; Legrand, A. P. High-Resolution ^{29}Si Solid-State NMR Study of Silicon Functionality Distribution on the Surface of Silicas. *Magn. Reson. Imaging* **1996**, *14*, 911−913.
(40) Ng, K. L.; Chadwick, D.; Toseland, B. A. Kinetics and Modelling of Dimethyl Ether Synthesis from Synthesis Gas. *Chem. Eng. Sci.* **1999**, *54*, 3587−3592.
(41) Mores, D.; Kornatowski, J.; Olsbye, U.; Weckhuysen, B. M. Coke Formation during the Methanol-to-Olefin Conversion: In Situ Microspectroscopy on Individual H-ZSM-5 Crystals with Different Brønsted Acidity. *Chem.—Eur. J.* **2011**, *17*, 2874−2884.
(42) Hereijgers, B. P. C.; Bleken, F.; Nilsen, M. H.; Svelle, S.; Lillerud, K.-P.; Bjørgen, M.; Weckhuysen, B. M.; Olsbye, U. Product Shape Selectivity Dominates the Methanol-to-Olefins (MTO) Reaction over H-SAPO-34 Catalysts. *J. Catal.* **2009**, *264*, 77−87.
(43) Tian, P.; Wei, Y.; Ye, M.; Liu, Z. Methanol to Olefins (MTO): From Fundamentals to Commercialization. *ACS Catal.* **2015**, *5*, 1922−1938.
(44) Catizzone, E.; Migliori, M.; Purita, A.; Giordano, G. Ferrierite vs. γ-Al_2O_3: The superiority of zeolites in terms of water-resistance in vapour-phase dehydration of methanol to dimethyl ether. *J. Energy Chem.* **2019**, *30*, 162−169.
(45) Guisnet, M.; Costa, L.; Ribeiro, F. R. Prevention of Zeolite Deactivation by Coking. *J. Mol. Catal. A: Chem.* **2009**, *305*, 69−83.
(46) Xie, B.; Zhang, H.; Yang, C.; Liu, S.; Ren, L.; Zhang, L.; Meng, X.; Yilmaz, B.; Müller, U.; Xiao, F.-S. Seed-Directed Synthesis of Zeolites with Enhanced Performance in the Absence of Organic Templates. *Chem. Commun.* **2011**, *47*, 3945−3947.
(47) Fu, T.; Chang, J.; Shao, J.; Li, Z. Fabrication of a Nano-Sized ZSM-5 Zeolite with Intercrystalline Mesopores for Conversion of Methanol to Gasoline. *J. Energy Chem.* **2017**, *26*, 139−146.
(48) Wang, N.; Sun, W.; Hou, Y.; Ge, B.; Hu, L.; Nie, J.; Qian, W.; Wei, F. Crystal-Plane Effects of MFI Zeolite in Catalytic Conversion of Methanol to Hydrocarbons. *J. Catal.* **2018**, *360*, 89−96.
(49) Zhong, J.; Han, J.; Wei, Y.; Xu, S.; He, Y.; Zheng, Y.; Ye, M.; Guo, X.; Song, C.; Liu, Z. Increasing the Selectivity to Ethylene in the MTO Reaction by Enhancing Diffusion Limitation in the Shell Layer of SAPO-34 Catalyst. *Chem. Commun.* **2018**, *54*, 3146−3149.

https://doi.org/10.1021/acsomega.2c01539
ACS Omega 2022, 7, 21654−21663